INT. J. NUM. METH. HEAT FLUID FLOW, VOL. 5, 907–921 (1995)

A FINITE ELEMENT ENTHALPY TECHNIQUE FOR SOLVING COUPLED NONLINEAR HEAT CONDUCTION/ MASS DIFFUSION PROBLEMS WITH PHASE CHANGE

R. L. McADIE, J. T. CROSS, R. W. LEWIS AND D. T. GETHIN

Institute for Numerical Methods in Engineering, University of Wales, Swansea, UK

ABSTRACT

A rigorous Finite Element (FE) formulation based on an enthalpy technique is developed for solving coupled nonlinear heat conduction/mass diffusion problems with phase change. The FE formulation consists of a fully coupled heat conduction and solute diffusion formulation, with solid-liquid phase change, where the effects of pressure and convection are neglected. A full enthalpy method is employed eliminating singularities which result from abrupt changes in heat capacity at the phase interfaces. The FE formulation is based on the fixed grid technique where the elements are two dimensional, four noded quadrilaterals with the primary variables being enthalpy and average solute concentration. Temperature and solid mass fraction are calculated on a local level at each integration point of an element.

A fully consistent Newton–Raphson method is used to solve the global coupled equations and an Euler backward difference scheme is used for the temporal discretization. The solution of the enthalpy-temperature relationship is carried out at the integration points using a Newton–Raphson method. A secant method employing the *regula falsi* technique takes into account sudden jumps or sharp changes in the enthalpy-temperature behaviour which occur at the phase zone interfaces. The Euler backward difference integration rule is used to calculate the solid mass fraction and its derivatives.

A practical example is analysed and results are presented.

KEY WORDS Finite element Heat conduction/diffusion Phase change Enthalpy method

INTRODUCTION

Many phase change problems encountered in the material processing industry are not only heat conduction dependent but are also influenced by the mass diffusion of the material constituents, where the two processes are coupled by the phase change mechanism. This phase change mechanism is, in turn, dependent on the local temperature and constituent concentration fields. Depending on the process, this mechanism can be governed by the equations of state (i.e. the phase diagram) where local thermodynamic equilibrium with respect to the material constituents is assumed – this is the case for most numerical models[1,2,3].

Different models representing the phase change process on the microscopic level have been developed; the lever rule model, where local thermodynamic equilibrium with respect to the material constituents is assumed in both the liquid and solid phases ('*equilibrium model*') and the Scheil model, where solid constituent diffusion is assumed to be negligible and only the constituent concentration in the liquid phase is at thermodynamic equilibrium ('*non-equilibrium*

0961-5539/95/100907-15$2.00

Received February 1994

model'). The type of model chosen not only affects the local phase change description but also affects the global variations in constituent concentration and temperature. The solid mass fraction, which is used as a measure of phase change, is therefore a function of temperature and average constituent concentration. If the global conservation equations are cast in a continuum form, the material constitutive and thermodynamic coefficients will, in turn, be functions of solid mass fraction. Therefore, what happens on a global level, governed by the continuum conservation equations, affects what happens on a local level, governed either fully or partially by the equations of state, and *vice-versa*. This results in a tightly coupled system of equations which describe the process.

Typical industrial processes that would be described by this set of equations are, among others, the alloy solidification process, the freezing or melting of solutions (e.g. desalination of water) and industrial diamond synthesis. It is appreciated that in some of these processes fluid convection plays a dominant role but the model described in this work is considered as a first step in modelling the particular process.

Depending on the material and process the phase change can be discrete, take place over a region (i.e. mushy phase change) or both. Different numerical techniques have been used to tackle these phase change problems. The front tracking technique is used for discrete phase change where an accurate description of the phase interface is required[4,5]. Conversely, the fixed grid method is preferred for diffuse mushy or mushy/discrete phase change. Some advantages of the fixed grid method are that it lends itself to easy implementation of continuum based formulations and it is computationally inexpensive when compared to the front tracking scheme. Much finite volume work in the field of alloy solidification has been conducted using the fixed grid continuum approach[2,3,6]. In contrast, little work in the finite element field has been published, besides that of Porier and Heinrich[7]. This paper therefore presents a mathematically rigorous fixed grid finite element formulation using an enthalpy technique to model the coupled phase change problem.

PROBLEM DEFINITION

The global conservation equations are that of energy (Fourier's law) and the conservation of solute (Fick's law) which are expressed as:

$$\rho C_p \frac{\partial T}{\partial t} = \nabla \cdot \boldsymbol{K} \nabla T + Q_H \tag{1}$$

and

$$\rho \frac{\partial \bar{C}}{\partial t} = \nabla \cdot \rho \boldsymbol{D} \nabla C^L + Q_C \tag{2}$$

respectively.

Both essential and natural boundary conditions are defined on different parts of the boundary of the domain. The essential boundary condition prescribes a given temperature g_H and/or a given solute concentration g_C which may depend on both position and time. The natural boundary condition can be described as a heat flux h_H and/or solute flux h_C. The heat flux h_H may depend on temperature, position and time, and can constitute an applied heat flux, radiative flux or convective flux. The solute flux h_C may depend on solute concentration, position and time, and constitutes an applied solute flux.

The internal heat generation Q_H is expressed as $Q_H = Q_H(T, x, t)$ and the solute source Q_C is expressed as $Q_C = Q_C(\bar{C}, x, t)$.

The material properties vary according to the phase of the material. The material is considered to have a maximum of three phases (i.e. solid, liquid and mush) at any one time. The

thermodynamic coefficients (effective specific heat C_p), the constitutive coefficients (conductivity K, and diffusivity D) and density ρ of the phase mixture are expressed in terms of a lever rule with respect to the solid mass fraction ϕ, with the exception of conductivity, which is expressed in terms of the phase volume fraction g^α where α represents solid (S) or liquid (L) phase. These properties allow a nonlinear dependence on temperature T and average solute concentration $\bar{C}$.

A summary of the material properties defining the phase mixture follows.

(a) The solid mass fraction is expressed as,

$$\phi = \phi(T, \bar{C}, x, t) = \begin{cases} 1 & \text{solid region} \\ 0 < \phi < 1 & \text{mushy region} \\ 0 & \text{liquid region} \end{cases}$$

(b) The effective specific heat of the phase mixture C_p is expressed as,

$$C_p = C_{p_0} - L\partial\phi/\partial T \tag{3}$$

where C_{p_0} is the lever rule specific heat of the phase mixture and is expressed as,

$$C_{p_0} = \phi C_p^S(T, x, t) + (1 - \phi)C_p^L(T, x, t) \tag{4}$$

and L is the latent heat (enthalpy of fusion), which is expressed as,

$$L = \int_{T_{ref}}^{T} (C_p^L(\tau, x, t) - C_p^S(\tau, x, t))\, d\tau + \Delta H_{ref}^f \tag{5}$$

where $C_p^S = C_p^S(T, x, t)$ is the specific heat of the solid, $C_p^L = C_p^L(T, x, t)$ is the specific heat of the liquid and ΔH_{ref}^f is the heat of formation of the liquid alloy which is constant. Dependency on the solute concentration of C_p^α in both phases are ignored.

(c) The average solute concentration of the phase mixture is expressed as,

$$\bar{C} = \phi\bar{C}^S + (1 - \phi)\bar{C}^L \tag{6}$$

where $\bar{C}^S$ is the average solute concentration in the solid and is expressed for the case of zero local solid diffusion by $\bar{C}^S = \frac{1}{\phi}\int_0^\phi C^S(f^S)\, dV^S$, and for the local solid diffusion case as $\bar{C}^S = C^S$ where $C^S = C^S(T, x, t)$ in the mushy region and $C^S = \bar{C}(x, t)$ in the solid. The term $\bar{C}^L$ is the average solute concentration of the solute in the liquid, where $\bar{C}^L = C^L$, which is expressed in the mushy region as $C^L = C^L(T, x, t)$ and in the liquid region as $C^L = \bar{C}(x, t)$. Complete solute mixing is assumed within the liquid phase and undercooling is neglected. As a result, the dendrite tips are located at the equilibrium liquidus temperature.

(d) The phase mixture density ρ is expressed as,

$$\rho = g^S\rho_*^S + g^L\rho_*^L \tag{7}$$

where $g^S = (\rho/\rho_*^S)\phi$ is the solid volume fraction, $g^L = (\rho/\rho_*^L)(1 - \phi)$ is the liquid volume fraction, ρ_*^S is the actual solid density and ρ_*^L is the actual liquid density. Note that the Oberbeck–Boussinesq approximations are used where it is assumed that ρ is constant (except in the buoyancy terms for the fluid flow case). To maintain phase mixture saturation, solid and liquid densities are assumed to be equal, therefore $\rho_*^S = \rho_*^L = \text{constant}$. From these assumptions therefore, $g^S = \phi$ and $g^L = (1 - \phi)$.

(e) The conductivity of the phase mixture is expressed as,

$$\boldsymbol{K} = g^S\boldsymbol{K}^S(T, \bar{C}, x, t) + g^L\boldsymbol{K}^L(T, \bar{C}, x, t) \tag{8}$$

where $\boldsymbol{K}^S$ is the conductivity tensor for the solid and $\boldsymbol{K}^L$ is the conductivity tensor for the liquid. Note that $\boldsymbol{K}^\alpha$ is allowed to be anisotropic although symmetry is assumed[8].

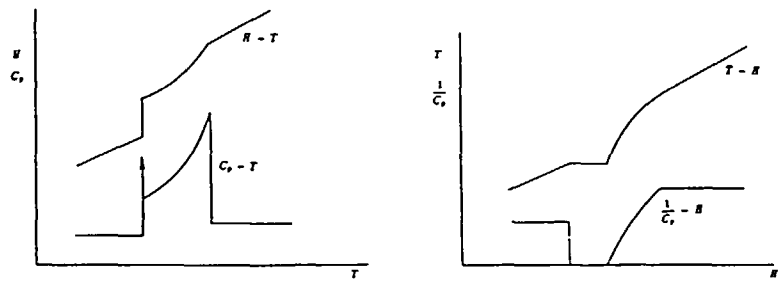

Figure 1 Enthalpy, specific heat, temperature relationships

(f) The diffusivity of the phase is expressed as,

$$D = \phi D^S(T, \bar{C}, x, t) + (1-\phi)D^L(T, \bar{C}, x, t) \tag{9}$$

where D^S is the diffusivity of the solid and D^L is the diffusivity of the liquid. It is assumed that the solid diffusion is zero, therefore $D^S = 0$.

The enthalpy approach

In the phase change region the specific heat C_p experiences Dirac-delta behaviour (*Figure 1*) which leads to significant numerical difficulties when trying to solve the conservation of energy equation. To circumvent this difficulty, enthalpy is introduced into the conservation equation (1) to give,

$$\rho \frac{\partial H}{\partial t} = \nabla \cdot \boldsymbol{K} \nabla T + Q_H \tag{10}$$

By rewriting the rate term in (10), in terms of enthalpy, numerical difficulties are only avoided when a non-discrete phase change takes place where the $T-H$ curve is a smooth function throughout the domain. However, as illustrated in *Figure 1*, the $T-H$ curve exhibits a discontinuity at the eutectic point of an alloy or at the melting temperature of a pure substance. Therefore the enthalpy becomes multi-valued, making the accurate solution of equation (10) very difficult and energy conservation cannot be ensured. If enthalpy is chosen as the field variable, rather than temperature, the function becomes single valued and this problem can be overcome with the energy being totally conserved. From *Figure 1*, it is clear that the $H-T$ curve experiences no discontinuity and also $\dfrac{\partial T}{\partial H}$, which is $\dfrac{1}{C_p}$, is zero in the discrete phase change region. Equation (10) expressed in terms of enthalpy is, therefore,

$$\rho \frac{\partial H}{\partial t} = \nabla \cdot \boldsymbol{K} \nabla T(H) + Q_H = \nabla \cdot \frac{\boldsymbol{K}}{C_p} \nabla H + Q_H \tag{11}$$

where the enthalpy for the phase mixture is expressed as,

$$H = \phi H^S + (1-\phi)H^L \tag{12}$$

where

$$H^S = H^S(T(H), x, t) = \int_{T_{ref}}^{T(H)} C_p^S(\tau, x, t)\, d\tau \tag{13}$$

and

$$H^L = H^L(T(H), x, t) = \int_{T_{ref}}^{T(H)} C_p^L(\tau, x, t)\, d\tau + \Delta H_{ref}^f \tag{14}$$

The advantage in using this enthalpy formulation is that it is characterized by a strictly decreasing or increasing enthalpy for solidification or melting respectively. It must be noted that even when using the full enthalpy approach the discontinuity which is implicit in the formulation cannot be correctly modelled using the fixed grid finite element formulation. Standard finite elements cannot handle a discontinuity within the elements and the jump in enthalpy will be smeared over the element or elements depending on the solution scheme used. It is also clear that to model this jump condition reasonably a fine mesh would have to be used.

FINITE ELEMENT FORMULATION

In this section, the solution of the global conservation equations of energy and solute, using a fixed grid finite element approach, is discussed. First, the strong form of the initial boundary-value problem (IBVP) is defined. This leads to the weighted residual or weak form of the problem. Next, the Galerkin approximation is introduced which, along with an assumed spatial discretization, leads to the finite element matrix form of the problem. The finite element matrix equations are then temporally discretized. The solution of the resulting nonlinear matrix of equations motivates the development of iterative algorithms. Finally, the linear problem generated by the iterative algorithms is discussed.

STRONG FORM OF THE INITIAL BOUNDARY-VALUE PROBLEM

Problem domain

The problem is posed for a body occupying a spatial domain Ω, a finite region of $\Re^{N_{sd}}$ where $\Re$ is the set of real numbers and N_{sd} is the number of space dimensions. A general point in $\bar{\Omega}$ will be denoted as $x = \{x_i\}$, $i = 1, 2, \ldots, N_{sd}$ where $\bar{\Omega}$ denotes a closed domain, i.e. the total domain including boundaries. The closed domain $\bar{\Omega}$ is divided up into different subregions, with $\bar{\Omega} = \overline{\Omega^S \cup \Omega^L \cup \Omega^M}$ where $\Omega^S \subset \Re^{N_{sd}} \times \tau$ (*the solid region of the domain*), $\Omega^L \subset \Re^{N_{sd}} \times \tau$ (*the liquid region of the domain*), $\Omega^M = \overline{\Omega^S \cap \Omega^L}$ (*the phase change region of the domain*) and τ denotes time. The three subdomains Ω^S, Ω^L and Ω^M vary with time. When the width of Ω^M tends to zero a discrete phase change results between Ω^S and Ω^L. This is described as $\Omega^S \cap \Omega^L = \varnothing$, where $\varnothing$ denotes the empty set.

The boundary of Ω, denoted Γ, is assumed to be piecewise smooth. At almost every point on Γ there is a unique outward normal unit vector $n = (n_i)$, $i = 1, 2, \ldots, N_{sd}$. In addition, Γ can be subdivided into two disjoint sets, Γ_g and Γ_h. Thus Γ admits the following decomposition $\Gamma = \Gamma_g \cup \Gamma_h$ and $\varnothing = \Gamma_g \cap \Gamma_h$, where $\Gamma_g = \overline{\Gamma_{g^L} \cup \Gamma_{g^M} \cup \Gamma_{g^S}}$ and $\Gamma_h = \overline{\Gamma_{h^L} \cup \Gamma_{h^M} \cup \Gamma_{h^S}}$, where the superposed bar represents set closure.

The strong form

The IBVP describing the coupled heat conduction/mass diffusion phase change process is defined. Therefore the strong form (S) of the IBVP can thus be stated as follows.

Given ρ, C_P, $\boldsymbol{K}$, $\boldsymbol{D}$, g_H, g_C, h_H, h_C, T_0 and $\bar{C}_0$,

find

$$H: \bar{\Omega} \times [0, \tau] \rightarrow R^+, \text{ expressed in section entitled Problem definition}$$

and

$$\bar{C}: \bar{\Omega} \times [0, \tau] \rightarrow R^+, \text{ expressed in section entitled Problem definition}$$

such that the following coupled equations hold:

$$\rho \frac{\partial H}{\partial t} = \nabla \cdot \frac{\boldsymbol{K}}{C_p} \nabla H + Q_H \text{ on } \Omega \times]0, \tau[\tag{15}$$

and

$$\rho \frac{\partial \bar{C}}{\partial t} = \nabla \cdot \rho \boldsymbol{D} \nabla C^L + Q_C \text{ on } \Omega \times]0, \tau[\tag{16}$$

where the essential boundary conditions are,

$$H = g_H \text{ on } \Gamma_g \times]0, \tau[\tag{17}$$

and

$$\bar{C} = g_c \text{ on } \Gamma_g \times]0, \tau[\tag{18}$$

the natural boundary conditions are,

$$\boldsymbol{n} \cdot \left(\frac{\boldsymbol{K}}{C_p} \nabla H \right) = h_H = h_{f_1} + h_{conv} + h_{rad} \text{ on } \Gamma_h \times]0, \tau[\tag{19}$$

and

$$\boldsymbol{n} \cdot (\rho \boldsymbol{D} \nabla C^L) = h_C = h_{f_2} \text{ on } \Gamma_h \times]0, \tau[\tag{20}$$

and the initial conditions are,

$$H(x, 0) = h_0(x) \; \forall x \in \Omega \tag{21}$$

and

$$\bar{C}(x, 0) = \bar{C}_0(x) \; \forall x \in \Omega \tag{22}$$

WEIGHTED RESIDUAL FORM OF THE INITIAL BOUNDARY-VALUE PROBLEM

The 'weighted residual' or 'weak' form of (S) is generated by a suitable choice of solution and variational spaces and the application of the divergence theorem, Mitchell[9] and Strang[10].

In order to develop a weak formulation for the IBVP, a total solution and a variational space are defined. Let H and w_1 denote the enthalpy fields and $\bar{C}$ and w_2 denote the solute concentration fields. The solution space $\mathcal{S}$ is defined as $\mathcal{S} = \mathcal{S}_H \cup \mathcal{S}_C$ where $\mathcal{S}_H = \{H | H = g_H \text{ on } \Gamma_g$ with $H = H^L$ in Ω^L, $H = \phi H^S + (1 - \phi) H^L$ in Ω_M and $H = H^S$ in $\Omega^S\}$, and where $\mathcal{S}_C = \{\bar{C} | \bar{C} = g_C$ on Γ_g with $\bar{C} = C^L$ in Ω^L, $\bar{C} = \phi \bar{C}^S + (1 - \phi) C^L$ in Ω_M, and $\bar{C} = \bar{C}^S$ in $\Omega^S\}$.

The variational space $\mathcal{V}$ is defined as $\mathcal{V} = \mathcal{V}_H \cup \mathcal{V}_C$ where $\mathcal{V}_H = \{w_1 | w_1 = 0 \text{ on } \Gamma_g\}$ and $\mathcal{V}_C = \{w_2 | w_2 = 0 \text{ on } \Gamma_g\}$.

Note that $\mathcal{S}$ is time dependent due to its use of the g-type condition, while $\mathcal{V}$ is time independent.

The weak form

The weak form of the problem (W) is obtained by multiplying (15) and (21) by $w_1 \in \mathscr{V}_H$ and (16) and (22) by $w_2 \in \mathscr{V}_C$, integrating over Ω, applying the divergence theorem, and making use of the boundary conditions (17)–(20) to simplify the result. This yields weak form for the IBVP as follows:

Given ρ, C_p, K, D, g_H, g_C, h_H, h_C, H_0 and $\bar{C}_0$,

find

$$H: [0, \tau] \to \mathscr{S}_H$$

and

$$\bar{C}: [0, \tau] \to \mathscr{S}_C$$

such that for every $w_H \in \mathscr{V}_H$ and $w_C \in \mathscr{V}_C$

$$M_H(\dot{H}, w_H) + K_H(H, w_H) = F_H(Q_H, w_H) + \dot{H}_H(h_H, w_H) \text{ on }]0, \tau[\tag{23}$$

$$M_C(\dot{\bar{C}}, w_C) + K_C(C^L, w_C) = F_C(Q_C, w_C) + H_C(h_C, w_C) \text{ on }]0, \tau[\tag{24}$$

$$(H(x, 0) - H_0, w_H) = 0 \text{ on } \Omega \tag{25}$$

and

$$(\bar{C}(x, 0) - \bar{C}_0, w_C) = 0 \text{ on } \Omega \tag{26}$$

The operators M_H, K_H, F_H, H_H, M_C, K_C, F_C, H_C and $(\cdot, \cdot)$ are defined respectively as:

$$M_H(\dot{H}, w_H) = \int_\Omega \dot{H}(x, t) w_H(x) \, d\Omega \tag{27}$$

$$K_H(H, w_H) = \int_\Omega \nabla H(x, t) \cdot \frac{K(T(x, t)), \bar{C}(x, t), x, t)}{C_p(T(H(x, t)), \bar{C}(x, t), x, t)} \nabla w_H(x) \, d\Omega \tag{28}$$

$$F_H(H, w_H) = \int_\Omega Q_H(T(H(x, t)), x, t) w_H(x) \, d\Omega \tag{29}$$

$$H_H(h_H, w_H) = \int_{\Gamma_h} h_H(T(H(x, t)), x, t) w_H(x) \, d\Gamma \tag{30}$$

$$M_C(\dot{\bar{C}}, w_C) = \int_\Omega \dot{\bar{C}}(x, t) \rho(x) w_C(x) \, d\Omega \tag{31}$$

$$K_C(C^L, w_C) = \int_\Omega \nabla C^L \cdot \rho(x) D(T(H(x, t)), \bar{C}(x, t) \nabla w_C(x) \, d\Omega \tag{32}$$

$$F_C(Q_C, w_C) = \int_\Omega Q_C(\bar{C}(x, t), x, t) w_C(x) \, d\Omega \tag{33}$$

$$H_C(h_C, w_C) = \int_{\Gamma_C} h_C(\bar{C}(x, t), x, t) w_C(x) \, d\Gamma \tag{34}$$

$$(H, w_H) = H(x, t) w_H(x) \, d\Omega \tag{35}$$

and

$$(\bar{C}, w_C) = \bar{C}(x, t) w_C(x) \, d\Omega \tag{36}$$

Note that:

(a) given suitable smoothness conditions a solution of (S) is a solution (W), (S)⇔(W),
(b) $M_H(\dot{H}, w_H)$, $K_H(H, w_H)$, $M_C(\dot{\bar{C}}, w_C)$, $K_C(C^L, w_C)$, $(\bar{C}, w_C)$ and (H, w_H) are symmetric bilinear forms.

GALERKIN APPROXIMATION OF THE INITIAL BOUNDARY-VALUE PROBLEM

The Galerkin form is derived from the weak form by approximating the variational and solution spaces with finite-dimensional subspaces.

The Galerkin approximation uses a finite number of linear independent functions to span a subspace $\mathscr{V}^h$ and $\mathscr{S}^h$ where $\mathscr{V}^h \subset \mathscr{V}$ and $\mathscr{S}^h \subset \mathscr{S}$. We represent $\mathscr{V}^h$ as $\mathscr{V}^h = \mathscr{V}^h_C \cup \mathscr{V}^h_H$, where $\mathscr{V}^h_H = \{w^h_H | w^h_H = \sum_{A=1} N_A(x) d_A,\ w^h_H = 0 \text{ on } \Gamma_g\}$ and $\mathscr{V}^h_C = \{w^h_C | w^h_C = \sum_{A=1} N_A(x) \hat{d}_A,\ w^h_C = 0 \text{ on } \Gamma_g\}$, where $N_A, A = 1, 2, \ldots, n$, are linearly independent functions in $\mathscr{V}$ and d_A and $\hat{d}_A$ are constants.

Similarly, the approximation to the trial solution space $\mathscr{S}^h = \mathscr{S}^h_H \cup \mathscr{S}^h_C$, where $\mathscr{S}^h_H = \{H^h | H^h = v^h_H + g^h_H,\ v^h_H \in \mathscr{V}^h_H,\ g^h_H \in \mathscr{S}^h_H\}$ and $\mathscr{S}^h_C = \{C^h | v^h_C + g^h_C,\ v^h_C \in \mathscr{V}^h_C,\ g^h_C \in \mathscr{S}^h_C\}$.

The Galerkin form

The galerkin approximation (G) of the IBVP may therefore be stated as follows.

Given ρ, C_p, $\boldsymbol{K}$, $\boldsymbol{D}$, g_H, g_C, h_H, h_C, H_0 and $\bar{C}_0$, find

$$H^h = v^h_H + g^h_H \colon [0, \tau] \to \mathscr{S}^h_H$$

and

$$\bar{C}^h = v^h_C + g^h_C \colon [0, \tau] \to \mathscr{S}^h_C$$

such that for every $w^h_H \in \mathscr{S}^h_H$ and $w^h_C \in \mathscr{S}^h_C$,

$$M_H(\dot{v}^h_H, w^h_H) + K_H(v^h_H, w^h_H) = F_h(Q_H, w^h_H \tag{37}$$

$$+ H_H(h^h_H, w^h_H) - M_H(\dot{g}^h_H, w^h_H) - K_H(g^h_H, w^h_H) \text{ on }]0, \tau[\tag{38}$$

$$M_C(\dot{v}_C, w^h_C) + K_C(v^h_C, w^h_C) = F_H(Q_C, w^h_C) \tag{39}$$

$$+ H(h^h_C, w^h_C) - M_C(\dot{g}^h_C, w^h_C) - K_C(g^h_C, w^h_C) \text{ on }]0, \tau[\tag{40}$$

$$(v^h_H(x, 0), w^h_H) = (H_0 - g^h_H(x, 0)) \text{ on } \Omega \tag{41}$$

and

$$(v^h_C(x, 0), w^h_C) = (\bar{C}_0 - g^h_C(x, 0)) \text{ on } \Omega \tag{42}$$

FINITE ELEMENT MATRIX APPROXIMATION OF THE INITIAL BOUNDARY-VALUE PROBLEM

The finite element matrix equations are derived from the Galerkin form by defining the approximation of the variational and solution spaces based on a given spatial discretization.

A finite element basis for $\mathscr{S}^h$ and $\mathscr{V}^h$ is defined by using a finite number of linear independent functions $N_a(x)$ which span $\mathscr{S}^h$ and $\mathscr{V}^h$, thus we can write,

$$v^h_H(x, t) = \sum_{A \in n - n_g H} N_a(x) h_a(t) \colon [0, t] \to \mathscr{V}^h_H \tag{43}$$

$$v^h_C(x, t) = \sum_{A \in n - n_g C} N_a(x) c_a(t) \colon [0, \tau] \to \mathscr{V}^h_C \tag{44}$$

and

$$g_H^h(x, t) = \sum_{A \in n_e H} N_a(x) g_{H_a}(t) \colon [0, \tau] \to \mathscr{S}_H^h \tag{45}$$

$$g_C^h(x, t) = \sum_{A \in n_e C} N_a(x) g_{C_a}(t) \colon [0, \tau] \to \mathscr{S}_C^h \tag{46}$$

From (43), we see that a function in $\mathscr{V}_H^h$ may be represented in terms of a time-varying vector $\boldsymbol{h}$ of N_{EQ}^H components that are coefficients associated with shape functions. Similarly a function in $\mathscr{V}_C^h$ may be represented in terms of a time-varying vector $\boldsymbol{c}$ of N_{EQ}^C components that are coefficients associated with shape functions. Note that the time-dependent coefficients g_{H_a} and g_{C_a} are chosen so that g_H^h is a 'good' approximation of g_H and g_C^h is a 'good' approximation of g_C.

The finite element matrix form

The finite element matrix form (M) of the IBVP is:
Given ρ, C_p, $\boldsymbol{K}$, $\boldsymbol{D}$, g_H, g_C, h_H, h_C, H_0 and $\bar{C}_0$, find

$$\boldsymbol{h} \colon [0, \tau] \to \mathscr{R}^{N_{Eq}^H}$$

and

$$\boldsymbol{c} \colon [0, \tau] \to \mathscr{R}^{N_{Eq}^C}$$

such that

$$\boldsymbol{M}\dot{\boldsymbol{h}} + \boldsymbol{K}_H(\boldsymbol{h}, \boldsymbol{c}, t)\boldsymbol{h} = \boldsymbol{F}_H(\boldsymbol{h}, t) \tag{47}$$

$$\boldsymbol{M}\dot{\boldsymbol{c}} + \boldsymbol{N}_C(\boldsymbol{h}, \boldsymbol{c}, t) = \boldsymbol{F}_C(\boldsymbol{c}, t) \tag{48}$$

$$\boldsymbol{h}(0) = \boldsymbol{h}^0 \tag{49}$$

and

$$\boldsymbol{c}(0) = \boldsymbol{c}^0 \tag{50}$$

where $\boldsymbol{h}(t)$ and $\boldsymbol{c}(t)$ are respectively vectors of nodal enthalpy and solute concentration at time t, and $\boldsymbol{h}^0$ and $\boldsymbol{c}^0$ are a 'good' approximation to the exact initial enthalpy H_0 and $\bar{C}_0$, respectively.

TEMPORAL ALGORITHM

The semi-discrete matrix form (M) of the coupled nonlinear ordinary differential equations is discretized in terms of time where the real enthalpy $\boldsymbol{h}(t_n)$, the real solute concentration $\boldsymbol{c}(t_n)$ and their rate terms are approximated by discrete values $\boldsymbol{h}_n$ and $\boldsymbol{c}_n$, and, $\dot{\boldsymbol{c}}_n$ and $\dot{\boldsymbol{h}}_n$, respectively. The discrete solution times are given by $t_n = n\Delta t$, where Δt can be a constant or varying time step depending on the degree of nonlinearity of the problem.

Generalized trapezoidal rule

The time-integration method chosen is the generalized trapezoidal rule (T). Applying it to the matrix form of the problem (M) leads to the following time-integration scheme:
Given $\boldsymbol{M}$, $\boldsymbol{K}_H$, $\boldsymbol{F}_H$, $\boldsymbol{N}_C$ and $\boldsymbol{F}_C$, as in equations (47)–(48), find

$$\boldsymbol{h}_n,\ n \in \{0, \cdots N_{steps}\}$$

and

$$\boldsymbol{c}_n,\ n \in \{0, 1 \cdots N_{steps}\}$$

such that

$$M\dot{h}_{n+1} + K_H(h_{n+1}, c_{n+1}, t_{n+1})h_{n+1} = F_H(h_{n+1}, t_{n+1}) \tag{51}$$

$$M\dot{c}_{n+1} + N_C(h_{n+1}, c_{n+1}, t_{n+1}) = F_C(c_{n+1}, t_{n+1}) \tag{52}$$

$$h_0 = h^0 \tag{53}$$

$$c_0 = c^0 \tag{54}$$

$$h_{n+1} = h_n + \Delta t\{(1-\alpha)\dot{h}_n + \alpha\dot{h}_{n+1}\} \tag{55}$$

and

$$c_{n+1} = c_n + \Delta t\{(1-\alpha)\dot{c}_n + \alpha\dot{c}_{n+1}\} \tag{56}$$

where $\alpha = [0, 1]$.

In this algorithm α is chosen so that the solution will be unconditionally stable, as in most solidification problems the solution is sought over very long time periods compared to the stability limit for the explicit form of the operator (i.e. when $\alpha = 0$), Abaqus[11]. Of these algorithms, the central difference method pi.e. $\alpha = \frac{1}{2}$) has the highest accuracy. However, this method tends to produce oscillations in the early time solution. These oscillations are not present in the backward difference method (i.e. $\alpha = 1$). Thus the backward difference method is used.

NONLINEAR SOLUTION SCHEME

The iterative scheme proposed for solving the nonlinear algebraic problem is a variant of Newton–Raphson iteration, which makes use of the continuity of the temporal discretization. This predictor-corrector method makes use of a fully 'consistent' linearized operator to compute solution increments, which results in a non-symmetric linear equation system where quadratic convergence is ensured, Hughes[12].

Newton–Raphson iteration scheme

Obtain values h_{n+1} and c_{n+1} such that the residual $r(h_{n+1}, r_{n+1}) = 0$ where

$$r(h_{n+1}, c_{n+1}) = \begin{bmatrix} r_H(h_{n+1}, c_{n+1}) \\ r_C(h_{n+1}, c_{n+1}) \end{bmatrix} = \begin{bmatrix} 0 \\ 0 \end{bmatrix} = 0 \tag{57}$$

where

$$r_H(h_{n+1}, c_{n+1}) = M\left(\frac{h_{n+1} - h_n}{\Delta t}\right) + K_H(h_{n+1}, c_{n+1}, t_{n+1})h_{n+1} - F_H(h_{n+1}, t_{n+1}) \tag{58}$$

and

$$r_C(h_{n+1}, c_{n+1}) = M\left(\frac{c_{n+1} - c_n}{\Delta t}\right) + N_C(h_{n+1}, c_{n+1}, t_{n+1}) - F_C(c_{n+1}, t_{n+1}) \tag{59}$$

Using a Taylor series expansion about the exact solutions c_{n+1} and h_{n+1}, we may approximate the residual r at the values h^i_{n+1} and c^i_{n+1} and by ignoring higher order terms in the Taylor expansion, we may write,

$$\begin{bmatrix} \dfrac{\partial r_H}{\partial h} & \dfrac{\partial r_H}{\partial c} \\ \dfrac{\partial r_C}{\partial h} & \dfrac{\partial r_C}{\partial c} \end{bmatrix}_{\substack{h = h^i_{n+1} \\ c = c^i_{n+1}}} \begin{bmatrix} \Delta h^i_{n+1} \\ \Delta c^i_{n+1} \end{bmatrix} = \begin{bmatrix} -r_H(c^i_{n+1}, h^i_{n+1} \\ -r_C(c^i_{n+1}, h^i_{n+1}) \end{bmatrix} \tag{60}$$

The solution of this equation allows a better approximation to the exact solution, thus

$$c_{n+1}^{i+1} = c_{n+1}^{i} + \Delta c_{n+1}^{i} \tag{61}$$

and

$$h_{n+1}^{i+1} = h_{n+1}^{i} + \Delta h_{n+1}^{i} \tag{62}$$

In order to evaluate the residual and the Jacobian operator at the specific sampling point $\bar{\xi}(x)$, the mass fraction $\phi(\bar{\xi})$ and the temperature $T(\bar{\xi})$ have to be calculated from the given enthalpy and average solute concentration fields as follows: for time $n+1$ and for the ith global iteration, $H_{n+1}^{i}(\bar{\xi}) = \sum_{i=1}^{nnode} N_i(\bar{\xi})(h_i)_{n+1}^{i}$ and $\bar{C}_{n+1}^{i}(\bar{\xi}) = \sum_{i=1}^{nnode} N_i(\bar{\xi})(c_i)_{n+1}^{i}$.

These unknown variables, temperature $T(\bar{\xi})$ and solid mass fraction $\phi(\bar{\xi})$ at $\bar{\xi}(x)$, are termed the state variables of the problem. The state variables are based on the micromechanics of the phase change problem. Therefore, the state variables, will describe the phase change kinetics of the problem depending on the type of microscopic phase evolution model chosen.

The temperature $T(\bar{\xi})$ and solid mass fraction $\phi(\bar{\xi})$ are calculated using the temperature (T)-enthalpy (H) relationship (shown in *Figure 1*) coupled with the microscopic phase evolution model. This is based on the expression for the average solute concentration, equation (6). As the (T–H) relationship is unknown and the phase evolution model is not explicit, a predictor-corrector Newton–Raphson type algorithm is used. This is coupled with a trapezoidal integration scheme of the mass fraction evolution[13]. The (T–H) curve experiences sharp change in slope at phase interfaces. At these points, the Newton–Raphson method will not converge, so the secant method employing the *reguli falsi* technique is then used to obtain convergence (McAdie[13]).

NUMERICAL CONSIDERATIONS

To solve the equations which make up the residual vector and Jacobian matrix numerically, a Newton Cotes numerical integration scheme is chosen. This is because the sampling points are at the nodes of the element resulting in a diagonal mass matrix contribution to the Jacobian. This is equivalent to using a lumped mass method. In contrast, the Gaussian quadrature scheme, with sampling points positioned inside the element, would cause the mass matrix contribution to the Jacobian to be fully consistent. It has been found that oscillations, which appear in the solution when using a fully consistent mass matrix Jacobian contribution, do not occur when this matrix is lumped. It must be noted that a combination of the two schemes can also be used (i.e. Newton Cotes for the mass terms and Gaussian quadrature for the conductivity and diffusivity terms[11].

As the enthalpy solution is not smooth at the phase front low ordered linear elements are used, since better behaviour from higher-order elements cannot be expected in this case.

SOLIDIFICATION OF AN AL–SI INVESTMENT CASTING

A two-dimensional analysis of a cross-section of a thin walled aluminium alloy investment casting was made. The mould was made of a ceramic shell, which was preheated to the pouring temperature of the Al–Si (800°C). Once the metal was poured, the mould and casting were left to cool on a sand bed. A geometric description of the 2D cross-section, with the boundary conditions, is given in *Figure 2*. As it is symmetric, only half the cross-section was analysed.

The phase diagram for the Al–Si system is given in *Figure 3*. The alloy used is L99, composed of 93% Al and approximately 7% Si, and has the following material properties: density $\rho = \rho_S = \rho_L = 2700\ \mathrm{kg/m^3}$, latent heat $L = 3.975 \times 10^5\ \mathrm{J/kg}$, specific heat capacity $C_p = C_{p_S} = C_{p_L} = 1.196 \times 10^3\ \mathrm{Jkg^{-1}\,K^{-1}}$, conductivity $K = K_L = K_S = 226\ \mathrm{Wm^{-1}\,K^{-1}}$ and liquid diffusion coefficient $D_L = 4.8 \times 10^{-9}\ \mathrm{m^2\,s^{-1}}$. The material properties for the ceramic shell were

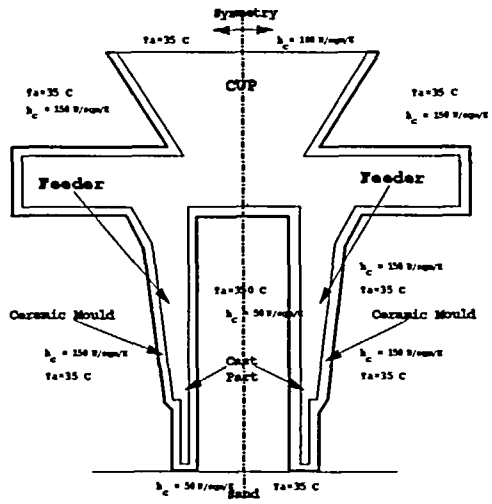

Figure 2 2D cross-section of a thin walled aluminium alloy investment casting

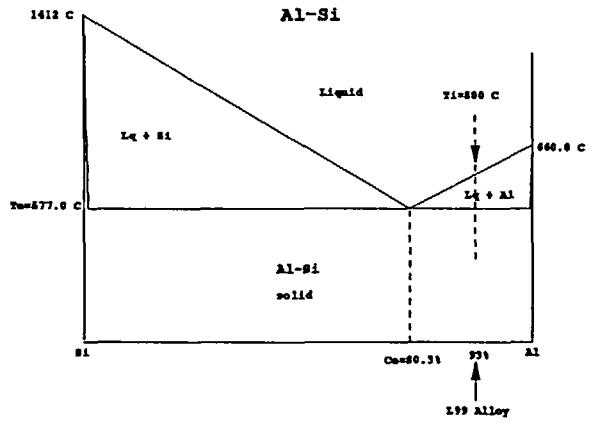

Figure 3 Al–Si alloy phase diagram

approximated by those of sand as the foundry had no thermal data for their ceramic. The assumed thermal properties are: density $\rho = 1830\,\text{kg/m}^3$, specific heat capacity $C_p = 0.9635 \times 10^3\,\text{Jkg}^{-1}\,\text{K}^{-1}$ and conductivity $K = 0.7325\,\text{Wm}^{-1}\,\text{K}^{-1}$. Radiation was an important mechanism for heat transfer across the boundary in this problem, but is expensive to calculate. Experiments were conducted, the results of which have been used in conjunction with inverse methods to obtain an equivalent heat transfer coefficient.

An unstructured mesh of 701 4-noded elements was used to solve the problem. This is shown, along with contours of temperature and solid mass fraction after 520 seconds, in *Figure 4*. The position of the mushy zone at this particular time can be seen to be around the centre of the thin section of the part. *Figure 5* gives a zoomed view of the boxed area, showing contours of

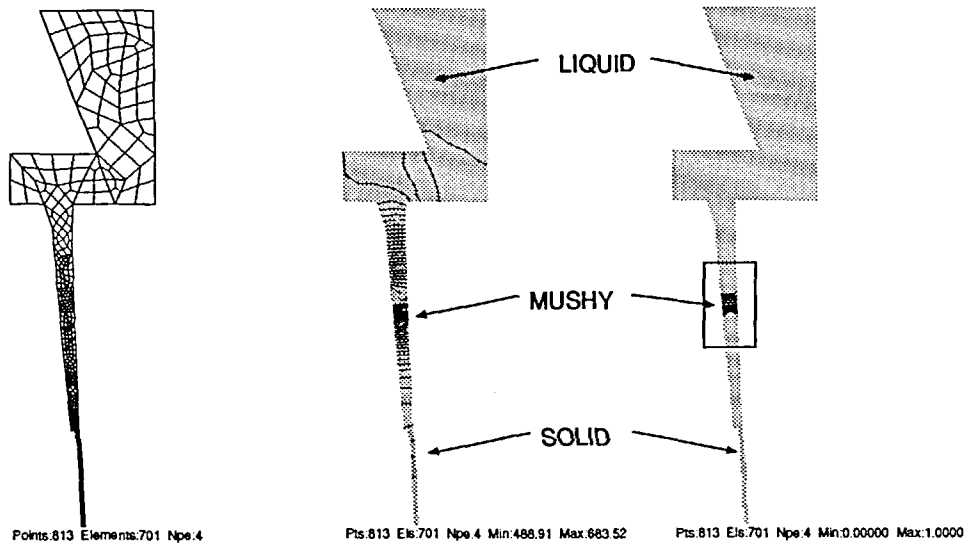

Figure 4 4-node mesh and distributions of temperature and solid mass fraction at 520 s

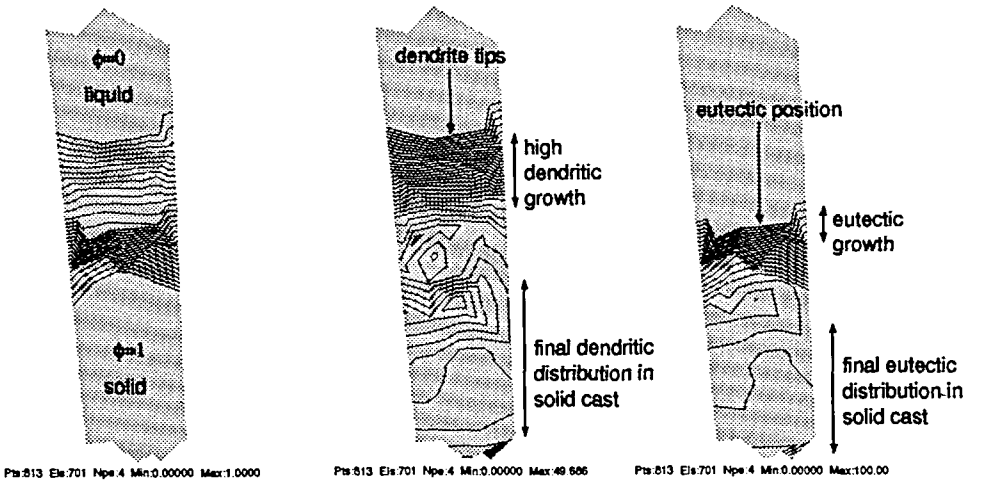

Figure 5 Solid mass fraction, ϕ, percentage dendritic and percentage eutectic at 520 s. Note that the eutectic is smeared because of element discretization

solid mass fraction and the percentages of dendritic and eutectic solidification. These clearly show the onset of dendritic solidification before the onset of eutectic solidification. The eutectic, although in principle a discrete position, is smeared across the width of an element.

The left side of *Figure 6* shows, at the end of solidification, the percentage of solidification that was dendritic, the remainder being eutectic. Note that the maximum value was 50% and the variation was considerable, suggesting an unstable crystal structure and, possibly, poor mechanical properties. The right side of *Figure 6* shows the predicted level of porosity, as

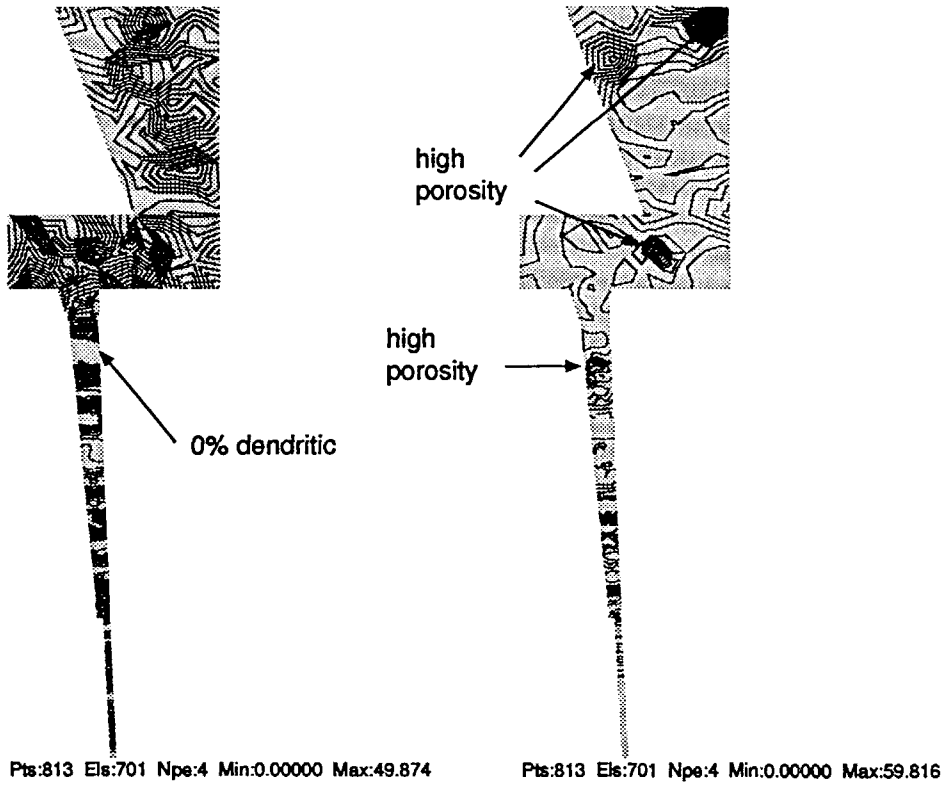

Figure 6 Percentage dendritic and Niyama porosity value at the end of solidification. Note that the region of high porosity coinciding with zero dendritic, also coincided with an area of porosity found in the actual cast part

calculated during the analysis using the Niyama criterion, also at the end of solidification. The higher values of porosity (>30) are found in the cup and in the cross-bar (which are of no real consequence) and around one-fifth of the way down the thin section. This coincides with a region where the model predicted zero dendritic solidification and, more importantly, the region where porosity was found in the actual casting.

CONCLUSION

A coupled nonlinear heat conduction/mass diffusion phase change formulation has been developed using an enthalpy technique for the fixed grid finite element method. The results clearly demonstrate the local/global coupling, in a problem of practical relevance. The enthalpy method is demonstrated to be proficient and accurate when dealing with this type of mushy/discrete phase change problem where energy conservation is ensured.

A real, investment casting problem has been analysed and defects arising in the casting have been successfully predicted.

REFERENCES

1 Bennon, W. D. and Incropera, F. P. A continuum model for momentum, heat and species transport in binary solid-liquid phase change systems – 1. Model formulation, *Num. Heat Transfer*, **30**, 2161–2170 (1987)
2 Bannon, W. D. and Incropera, F. P. Numerical analysis of binary solid-liquid phase change using a continuum model, *Num. Heat Transfer*, **13**, 277–296 (1988)
3 Voller, V. R., Brent, A. D. and Prakash, C. The modelling of heat, mass and solute transport in solidification systems, *Int. J. Heat Mass Transfer*, **32**, No. 9, 1719–1731 (1989)
4 Kececioglu, I. and Rubinsky, B. A continuum model for the propagation of discrete phase-change fronts in porous media in the presence of coupled heat flow, fluid flow and species transport processes, *Int. J. Heat and Mass Transfer*, **32**, 1111–1130 (1989)
5 Bonnerot, R. and Jamet, P. Numerical computation of the free boundary for the two dimension Stefan problem by space time finite elements, *J. Comput. Physics*, **25**, 163–181 (1977)
6 Prakash, C. and Voller, V. On the numerical solution of continuum mixture model equations describing binary solid-liquid phase change, *Num. Heat Transfer*, **15**, Part B, 171–189 (1989)
7 Poirier, D. R. and Heinrich, J. C. Simulations of thermosololutal convection in direction solidification, *Modelling of Casting and Welding and Advanced Solidification Processes VI*, edited by Piwonka, T. S., Voller, V. and Katgerman, L., TMS, 227–234 (1993)
8 Carslaw, H. S. and Jaeger, J. C. *Conduction of Heat in Solids*, Oxford University Press, Oxford (1959)
9 Mitchell, A. R. and Wait, R. *The Finite Element Method in Partial Differential Equations*, Wiley, New York (1977)
10 Strang, G. and Fix, G. J. *Analysis of the Finite Element Method*, Prentice-Hall, New Jersey (1973)
11 Hibbit, Karlson, and Inc. Sorenson, *ABAQUS Users Manual, Version 4.9*, Providence, Rhode Island, USA
12 Hughes, T. J. R. and Pister, K. S. Consistent linearization in mechanics of solids, *Computers and Structures*, **8**, 391–397 (1978)
13 McAdie, R. L. PhD Thesis: *Modelling of the Binary Alloy Solidification Process*, University of Cape Town, Cape Town, R.S.A. (1992)
14 McAdie, R. L., Martin, J. B. and Lewis, R. W. Finite element modelling of the binary alloy solidification process, *Modelling of Casting and Welding and Advanced Solidification Processes VI*, edited by Piwonka, T. S., Voller, V. and Katgerman, L., TMS, 169–177 (1993)